*Int. J. Electrochem. Sci.*, 17 **(2022)** Article Number: 220434, doi: 10.20964/2022.04.25

International Journal of
ELECTROCHEMICAL
SCIENCE
www.electrochemsci.org

# Europium Oxide Decorated on Graphitic Carbon Nitride as Electrochemical Sensor for Ultra-Selective Enhanced Electrocatalytic Detection of Azathioprine

*Balamurugan Karuppaiah[1], Jeyaraman Anupriya[1], Tse-Wei Chen[1,2], Shen-Ming Chen[1,*], Thirumurugan Senthilkumar[1], Syang-Peng Rwei[2,3], Xiaoheng Liu[4,*], Jaysan Yu[5]*

[1] Department of Chemical Engineering and Biotechnology, National Taipei University of Technology, No. 1, Section 3, Chung-Hsiao East Road, Taipei 106, Taiwan, ROC.
[2] Research and Development Center for Smart Textile Technology, National Taipei University of Technology, No.1, Section 3, Chung-Hsiao East Road, Taipei 106, Taiwan, ROC.
[3] Institute of Organic and Polymeric Materials, National Taipei University of Technology, Taiwan.
[4] Key Laboratory of Education Ministry for Soft Chemistry and Functional Materials, Nanjing University of Science and Technology, Nanjing 210094, China.
[5] Well Fore special wire corporation, 10, Tzu-Chiang 7rd., Chung-Li Industrial Park, Taoyuan, Taiwan
† *E-mail: smchen78@ms15.hinet.net (Shen-Ming Chen), xhliu@mail.njust.edu.cn (Xiaoheng Liu)

*Received:* 14 December 2021 / *Accepted:* 26 January 2022 / *Published:* 4 March 2022

The purpose of this article is to describe an effective and accurate electrochemical sensor based on Europium oxide (Eu-O)/graphitic carbon nitride (g-CN) nanocomposite towards the sensing and determination of the autoimmune depressive drug Azathioprine (AZP). EuO/g-CN nanocomposite was produced by using a superficial sonochemical technique. As demonstrated by impedance measurements, g-CN to the EuO lattice considerably low resisting property, which is advantageous for the electrochemical sensing process. Due to the unique aggregated coral like EuO nanoparticle on the flake-like g-CN, it shows excellent synergy and the electrode modified with EuO/g-CN demonstrated outstanding electrochemical behaviour for AZP sensing. The electrode modified with EuO/g-CN exhibited high sensitivity (0.410 µA $\mu M^{-1}$ $cm^{-2}$) and a detectable limit (8 nM), with high selectivity toward AZP. To demonstrate the sensor's utility, it was used to detect AZP in real sample, the determination of AZP was exhibited in biological fluids namely, human blood serum and urine samples.

**Keywords:** Azathioprine, Europium oxide, Graphitic carbon nitride, Nanocomposite, Electrochemistry.

## 1. INTRODUCTION

From purine based chemicals, Azathioprine (AZP) is a immunodepressive drug which used to treat leukemia caused during the transplantation of organs like kidney, and liver. Moreover, it was

reducing the immunological rejection rate of the organs during the transplantation [1]. In addition to that, AZP is used to cure the immunity deficiency diseases such as multiple sclerosis, bowel inflammation, autoimmune diseases, and lupus erythematosus. Meanwhile, the immunes system of the routine users was affected by the metabolized product (mercaptopurine) of AZP. Additionally, the following complications namely, bone marrow suppression, hair loss, nausea, rashes, hair loss, and fatigue were occurred during frequently usage of AZP. Moreover, the following tumours like lymphoma, leukaemia, and skin cancer may be developed during the long-term usage of AZP [1-4]. Due to the above facts, the unreliable technique was required to monitoring the AZP is an important. The AZN determination has been previously reported by using the traditional techniques like electrophoresis, high performance liquid chromatography, chemiluminesence, NMR spectroscopy, and surface enhance Raman spectroscopy [5-9]. The above said techniques need a more working procedure, very skilled person to operate the instruments, long-time to get results, high-cost instruments. Moreover, the selectivity of those techniques can be limited. Due to low costs, short analysis periods, and higher sensitivity, low detection limit, the electrochemical sensor has been recently demonstrated a high degree of benefits for the examination of any pharmaceutical analysis [10]. In that row, some electrochemical techniques had been reported for the electrochemical determination of azathioprine [3, 4, 11]. Meanwhile, due to the slow electrocatalytic activity of AZP, the suitable material is an important role towards the higher sensitivity and selectivity in AZP determination.

Rare earth (RE) materials have garnered considerable interest in a wide range of applications, including storage energy, superconductors, photonics, photochemical and electrochemical catalysis, heterogeneous catalysis, due to their high oxygen storage-release capacity (OSC), exceptional electronic constructions that include conversion approaches such as the 4-f shell, an indication of the atomic magnetic moment, and distinct coral structure [12-19]. Among them, europium oxide (EuO) being a rare earth-metal oxide, shows extremely vigorous redox features while used as a quasi-capacitor electrode. Hence, EuO might has a prospective application as electrochemical sensors due to their unique redox properties proceeding through CV at the electrode substance at varied absorptions to the target analyte. Likewise, individually value of the current strength corresponds to a distinct concentration of the target molecule [20]. When used in electrochemical sensors, transition metal doped RE oxides [21] or composite RE oxide with metal oxides [22] were reported accomplished of sensing various mineral ions and measuring various drugs [21,22]. As a result, the framework design of EuO rare earth metal oxide for enhancing the electrochemical active property may out to be interesting research.

Graphitic carbon nitride (g-CN) is a chemical and thermal stability material which has been recent addition to the family of carbon-based materials. Due to the presence of π-conjugated bonds between the covalently bonded carbon and nitrogen atoms, it has been polymerized through a π-conjugated bond and classified to polymeric material [23]. The occurrence of nitrogen atoms with non-bonding electrons on their surfaces provides an ideal active site for their interaction with a variety of chemical substances [24]. This interaction enables the use of certain polymeric materials as sensory components in the fabrication of very sensitive electrochemical sensors [25]. The following features like the synthesis procedure, chemical as well as thermal stability, metal free, less toxicity, high surface area, tunable electronic structure, enables the g-CN in different applications like photocatalysis, fluorescence

materials, and fuel cells [26-29]. Furthermore, we are unaware of any papers describing the use of europium oxide Coral structures on graphitic carbon nitride as electrode materials for biosensors.

In this work, we demonstrate an efficient sonochemical strategy for the synthesis of EuO/g-CN nanocomposite. Additionally, as-prepared nanocomposite was used as an electrode modification to develop a novel AZP sensor that is very sensitive and selective. Electrocatalytic sensing experiments confirms that as-prepared nanocomposite has excellent electrochemical performance for AZP sensing. The proposed sensor's analytical potential was also investigated by the sensor's utility, it was used to detect AZP in real sample analysis in human urine and blood serum.

## 2. EXPERIMENTAL TECHNIQUES

### *2.1. Chemicals and Instrumentations*

Europium nitrate pentahydrate ($Eu(NO_3)_3.5H_2O$), Azathioprine, Ammonia ($NH_3$), Urea ($NH_2$-CO-$NH_2$), Monosodium phosphate ($NaH_2PO_4$), Disodium phosphate ($Na_2HPO_4$), and other required materials were acquired in Sigma-Aldrich and they can be used as received without other modifications. Phosphate buffer solution (PBS, 0.1 M) was prepared by using $NaH_2PO_4$ and $Na_2HPO_4$ in distilled water.

Electrochemical analysis was performed using cyclic voltammetry (CV, CHI 1205C) and differential pulse voltammetry (DPV, CHI 900) techniques. Entire electrochemical analysis was carried out in nitrogen saturated 0.1 M PBS which contains conventional three electrodes namely, Glassy carbon electrode (GCE, working electrode), KCl saturated Ag/AgCl (Reference electrode), and platinum wire (Counter electrode). X-ray diffraction studies were conducted in XPERT PRO spectrometer (Cu-K radiation, = 1.5406. The potential functional groups present in the as-prepared materials were evidenced by FT-IR spectroscopy (FT-IR-6600). Structure, morphology, composition of elements was analyzed by FE-SEM coupled with EDX and HR-TEM (FE-SEM, quanta 250, FEG, Hitachi, Japan operated at 15 kV, HR-TEM; JEOL 2100F).

### *2.2. Preparation of EuO/g-CN nanocomposite*

#### *2.2.1. Sonochemical Synthesis of Coral-like EuO nanoparticle.*

In a sonication cell, 500 mg of europium nitrate pentahydrate was dissolved in 100 mL distilled water and the cell was connected to the sonicator horn. For 120 minutes at a steady temperature of 15-20 °C, a clean solution was sonicated by high-intensity ultrasound radiation. The pH of the reaction was maintained at 8 by dropwise adding 24 % (wt.) aqueous ammonia throughout sonication. The precipitate formed gradually, as ammonia was added drop-wise. Samples were washed thrice with double distilled water, centrifuged, and dried in a vacuum oven. Thus, the as-prepared materials were crystallized by heating a tiny portion of them in a boat alumina crucible at 700 °Cover 4 hours in the air [30].

*2.2.2. Preparation of g-CN flakes*

Bulk g-CN was produced using a modified version of the traditional urea pyrolysis process [22]. 10 g of urea was generally placed in a porcelain crucible afterward temperature increases from room temperature at a rate of 5°C/min. Following that, the temperature was controlled at 550°C for 4 hours and then subsequently cooled to room temperature to get bulk g-CN. Second, the 0.2 g bulk g-CN were ultrasonically dissolved in 20 mL water for 10 hours at 115 °C, washed and purified five times with distilled water, and then dissolved in double-distilled water and centrifuged (2000 rpm, 10 min) to separate the precipitation of large flakes, and then centrifuged again (10,000 rpm, 10 min) to get g-CN nanoflake precipitate for future usage.

*2.1.3. Preparation of EuO/g-CN nanocomposite*

For the preparation of EuO/gCN nanocomposite, 1g of g-CN and 2g of EuO were dissolved in aqueous media and then sonicated for an hour. After that, purification was done by washing this solution with water and ethanol. subsequently, the obtained product can be dried under a vacuum dried oven. **Scheme1** illustrates the synthesis of as-prepared EuO/g-CN nanocomposite.

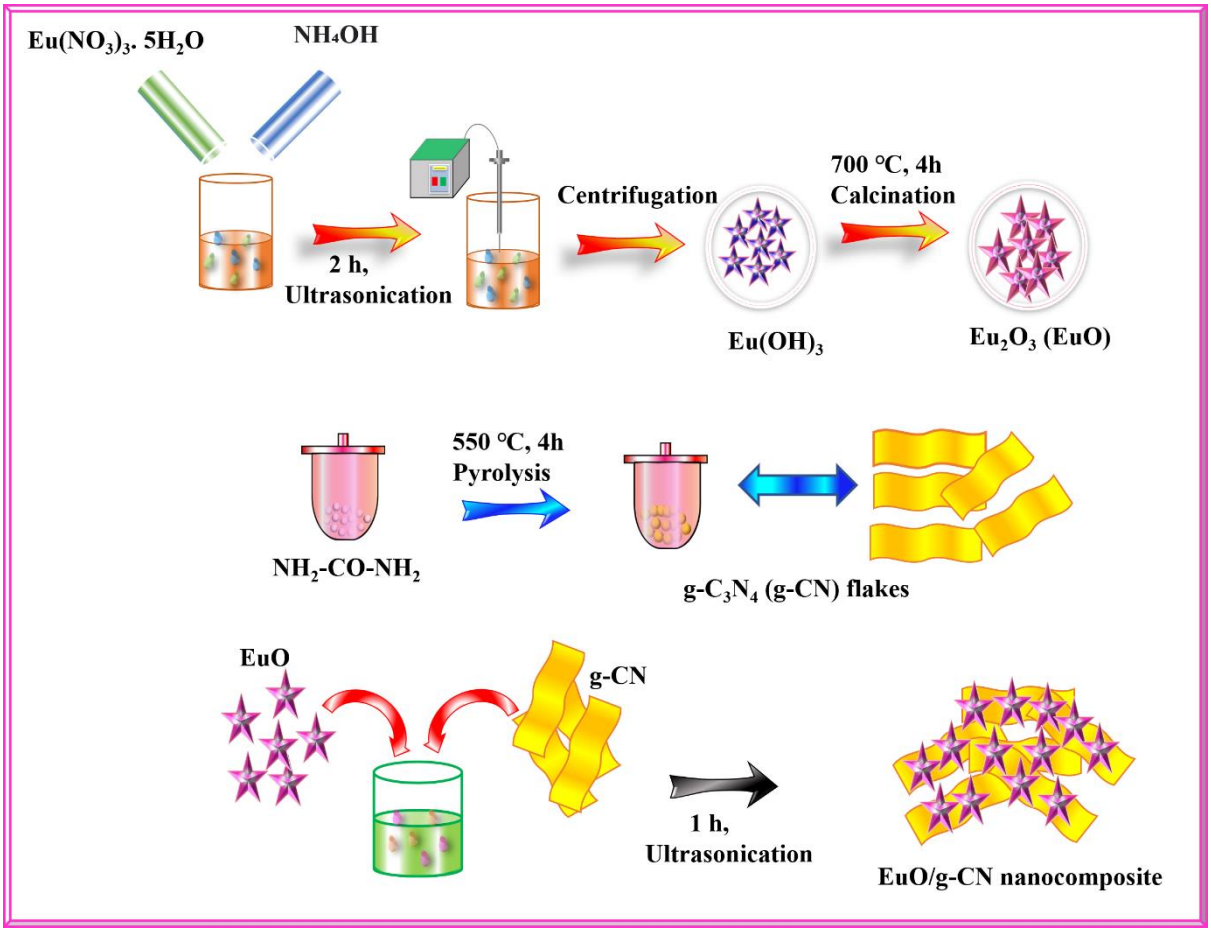


**Scheme 1.** Synthesis of as-prepared EuO/g-CN nanocomposite.

*2.2. Modification of GCE by EuO/gCN nanocomposite*

Prior to the GCE modification, a GCE has been polished by using 0.05g of alumina powder on a wet silicon carbide sheet. As a result, the pre-polished GCE has been used to modify the prepared electrocatalyst suspension. 5 mg of EuO/gCN nanocomposite was dispersed in distilled water and maintained at room temperature for 30 minutes under sonication. Followed that, 6 µL of the dispersed EuO/gCN dispersions were dropped cast on the functional electrode surface. The dryness of the EuO/gCN smooth surface was determined in order to evaluate the sensor's properties through additional electrochemical investigations. This approach was followed for all subsequent electrochemical/catalytic experiments.

## 3. RESULTS AND DISCUSSION

*3.1. XRD and FTIR analysis*

The powder X-ray diffraction techniques were employed to describe the crystalline phases of EuO/g-CN. Fig. 1A, indicate the XRD patterns of the EuO displays several high diffraction peaks at 16.3° (200), 28.3° (222), 31.6° (123), 32.9° (411), 41.1° (422), 45.6° (134), 47.5° (440), 50.5° (600) and 56.2° (622) respectively. The phase of EuO is identical to its cubic phase arrangement (space group-*Ia*3) and with JCPDS labelled number as 00-043-1008. Also, the XRD patterns of g-CN displays peaks at 13.06° (001), 17.6° (100), 27.6° (002) confirmed from JCPDS card number 00-087-1526. Moreover, the composite exhibited the g-CN peak at 27.6° was slightly shifted to 27.2° due to lattice parameters change was occurring. The composite was exhibit both g-CN and EuO peaks. It confirmed the creation of nanocomposite was completely pure. Hence, the formation of EuO, g-CN, and EuO/gCN nanocomposite was confirmed by XRD analysis.

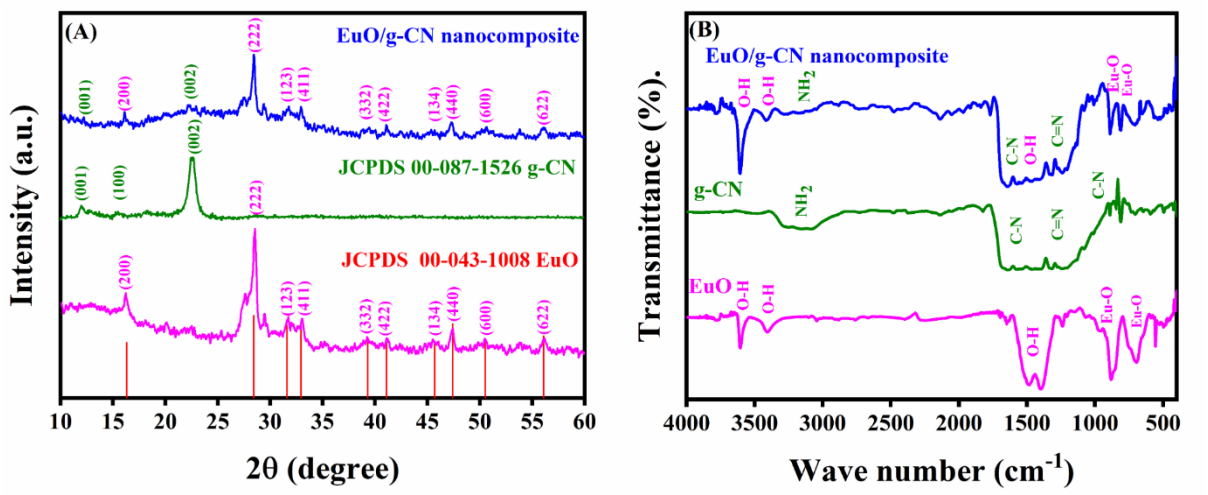


**Figure 1. (A)** XRD spectrum of EuO, g-CN, and EuO/gCN nanocomposite. (**B)** FTIR spectrum of EuO, g-CN, and EuO/gCN nanocomposite.

In addition, the functional group of the nanocomposite was established via FT-IR spectrum. FTIR spectra of g-CN, EuO, and EuO/gCN nanocomposite were displayed in Fig. 1B. The EuO was exhibit peaks at 3402 and 3601 $cm^{-1}$ are denoted as O-H stretching vibration of the water molecules [31]. The peaks are observed between 1100-1400 $cm^{-1}$ are denoted as O-H bending mode of water molecules [32]. The metal oxide was exhibit two peaks at 701 and 872 $cm^{-1}$ [33]. g-CN was exhibiting more peaks. The wide band appeared at 1570–1450 $cm^{-1}$ are allocated to C-N vibration, while the tri bands appeared at 1250, 1320, and 1430 $cm^{-1}$ were designated to vibration of C=N stretching. The peak at 810 $cm^{-1}$ resembles to condensed CN heterocycles were present in the triazine ring. A wide absorption band among 3145 and 3510 $cm^{-1}$ is reliable with the stretching peaks of $–NH_2$ or =NH groups, which corresponds to the uncondensed amine groups [34, 35, 36]. Finally, the composite was exhibit very well both material and carbon source peaks. It confirmed that the very well distribution of functional group was presented in the prepared nanocomposite.

### *3.2. Morphological Investigations*

Next, the morphological feature, the nanocomposite was examined and the results were portrayed in Fig. 2. The FE-SEM pictures of g-CN is included with the characteristic flakes-like morphology (Fig. 2A, B).

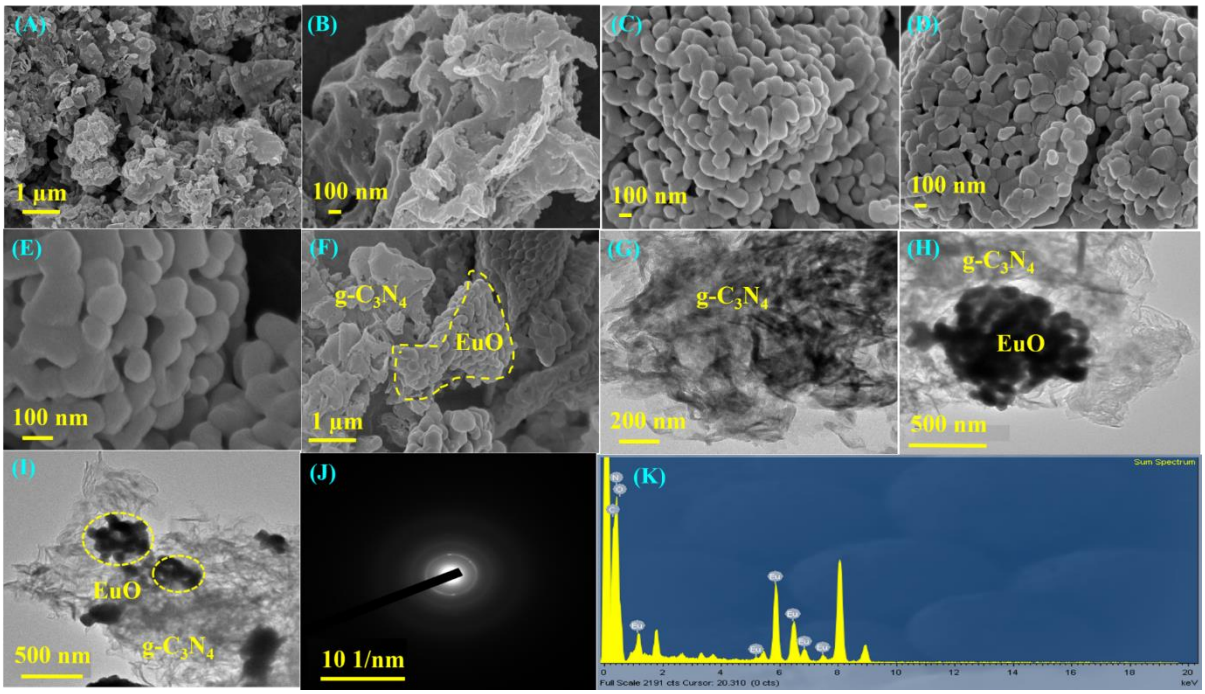


**Figure 2. (A-B)** 1µm and 100 nm FE-SEM image of the g-CN, **(C-E)** 100 nm FE-SEM image of EuO, **(F)** 1µm FE-SEM image of EuO/g-CN nanocomposite, and **(G)** HR-TEM image of g-CN at 200 nm **(H-I)** HR-TEM image of EuO/g-CN nanocomposite at 500 nm. **(J)** SAED pattern of EuO/g-CN nanocomposite. **(K)** EDX image of EuO/g-CN nanocomposite.

In FE-SEM high magnification and low magnification images exhibits the uniformed aggregated coral-like EuO nanoparticles and which was displayed in Fig. 2 C-E. Nevertheless, the FE-SEM pictures of EuO/g-CN nanocomposite displays the presence of aggregated coral-like EuO nanoparticles, it was well distributed on the flakes of g-CN (Fig. 2F). The size of the nanoparticle was ±100 nm. As a result, good electrostatic interface between g-CN flakes and EuO nanoparticles is probably stabilizing them in the nanocomposite form.

The HR-TEM figure of EuO and EuO/g-CN nanocomposite is exposed in Fig. 2G-I. The HR-TEM figure of EuO displays well aggregated coral like nano particles (Fig. 2G). Nevertheless, the HR-TEM figure of EuO/g-CN exposes the uniform spreading of several nanoparticles that are decorated by flakes like morphology, as probable for EuO/g-CN nanocomposite. Moreover, FE-SEM results and HR-TEM examines likewise indicate the effective construction of EuO/g-CN nanocomposite (Fig. 4G, H). The selected area diffraction (SAED) pattern (Fig. 2J) displays the slightly spots forming a ring like appearance, which refers to the amorphous nature and purity of EuO/g-CN nanocomposite. Fig. 2K shows the EDX analysis of Eu, C, N, and O elements were confirmed their presence in the nanocomposite having weight percentages of 16.6, 29.2, 42.6, and 11.6 %.

### *3.3. XPS analysis of EuO/g-CN nanocomposite*

XPS was used to further characterize the formation and surface electronic states of as-synthesized EuO/g-CN nanocomposite, and the corresponding high-resolution XPS spectra for Eu, O, C, and N are presented in Fig. 3. In the core level XPS spectra of Eu, two strong peaks at binding energies of 147.9 and 140.09 eV were found, which are attributed to a typical peak of $Eu^{3+}$ for $4d_{3/2}$ and $4d_{5/2}$ (Fig. 3B) [37]. Additionally, the core level XPS spectrum of O 1s reveals two peaks at 536 and 534 eV, indicating that the lattice oxygen was coupled to EuO [38]. The C 1s spectrum in Fig. 3D resolved into three peaks at 286, 290.3, and 294 eV, represents the presence of C–C or O=C bands, carboxyl carbon (O=C–O), and C-N bonds, respectively [25]. Furthermore, the core level N 1s resolution revealed two deconvolution peaks consuming binding energies of 401.1 and 403.1 eV (Fig. 3E), indicating that the samples exhibited two distinct forms of N bonding. Due to inadequate condensation during the heat polymerization procedure, one peak at 401.1 eV was recognized as the terminus amino group (C–N–H). The modest peak at 403.1 eV was caused by the successful synthesis of g-$C_3N_4$, which positively charged the g-$C_3N_4$ heterocycles, which was consistent with our zeta potential data [26]. By way of a result, the structural characterization approaches uneventfully confirm the formation of EuO/g-CN nanocomposite. The synergy among the prepared composites can result in an enhanced density of electrochemical surface sites, applying for its use as an active sensing material for environmental control.

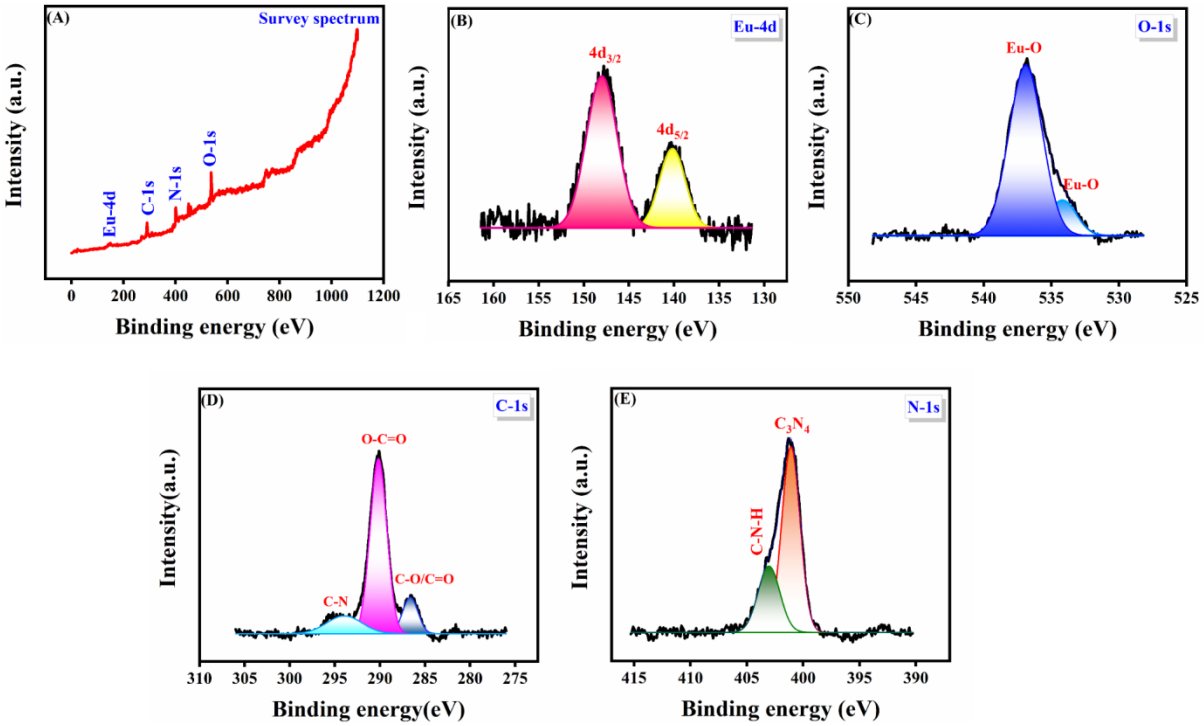


**Figure 3.** XPS spectrum of EuO/g-CN composite (**A**) Survey spectrum, (**B-E**) Core level spectra of Eu 4d, O 1s, C 1s, and N 1s.

*3.4. Electrochemical Impedance Spectral (EIS) Studies*

To investigate the modified electrode's electron transfer (interfacial) performance, EIS measurements were made (Fig. 4A). As shown in Fig. 4A, Nyquist plots (impedance curves) of bare GCE, EuO/GCE, g-CN/GCE, and EuO/g-CN/GCE were measured in 0.1 M KCl with 5 mM $[Fe(CN)6]^{3-/4-}$. In Nyquist plots, the semicircle region represents results from charge-transfer limitations, whereas the linear section represents diffusion-limited processes. The width of the semicircle specify the electrode's charge-transfer resistance ($R_{ct}$). At bare GCE, the expected impedance ($R_{ct}$) is 520 Ω, suggesting an extremely high impedance. The EuO/GCE semicircle diameter fell substantially, and the predicted charge-transfer resistance was 333Ω, indicating that EuO increased the electrochemical probe's diffusion. This could be related to EuO high conducting properties and paramagnetic nature. Thus, the charge-transfer resistance ($R_{ct}$) was significantly reduced to 235 Ω at g-CN/GCE, revealing that the high specific surface area as well as electron-hole nature of g-CN nano flakes. Finally, EuO/g-CN/GCE had an incredibly low impedance ($R_{ct}$) at 140 Ω due to EuO occupying the electron transfer pathway at the g-CN flakes. These results demonstrated that incorporating g-CN into the EuO lattice significantly increased the ionic conductivity of the EuO/g-CN/GCE system.

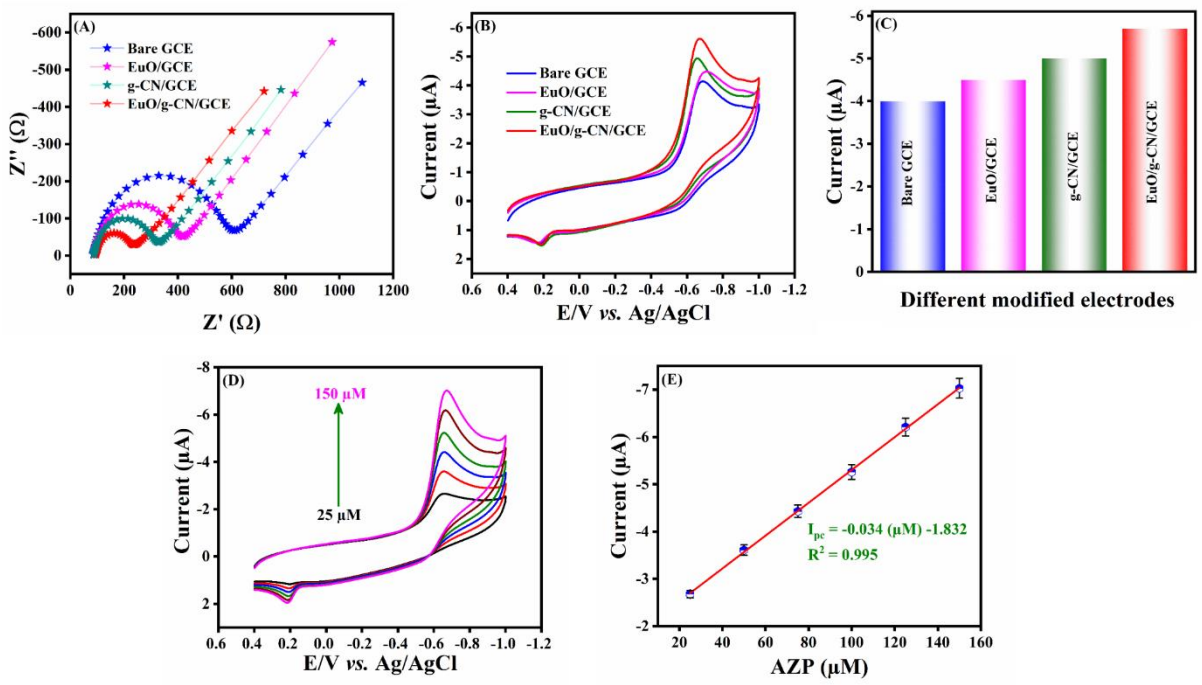


**Figure 4. (A)** Nyquist plots of unmodified GCE, modified GCE such as EuO/GCE, g-CN/GCE, and EuO/g-CN/GCE in 0.1 M of KCl containing 5 mM of $[Fe(CN)_6]^{3-/4-}$ **(B)** CVs of 100 µM AZP at modified electrodes in 0.1 M PB (pH 7.0) and a sweep rate of 50 mV/s. **(C)** Bar diagram of current response of AZP with respect to the modified electrodes. **(D)** CV histograms on EuO/g-CN/GCE in the existence of different amount of AZP (25-150 µM) in 0.1 M PB (pH 7.0). **(E)** Correlation plot between reduction current *vs*. AZP concentration.

### *3.5. Electrocatalytic Reduction of AZP at EuO/g-CN/GCE*

To evaluate the electrocatalytic response at EuO/g-CN/GCE towards the sensing of AZP, CVs were performed. The CVs for bare GCE, EuO/GCE, g-CN/GCE, and EuO/g-CN/GCE were determined in $N_2$ purged 0.1 M PBS (pH 7) which contains AZP (100 µM) and a sweep rate of 50 mV $s^{-1}$, as shown in Fig. 4B. The lack of reduction peak indicates that the bare GCE has a very low electrochemical performance for 100 µM AZP, demonstrating that the bare GCE have a limited electrocatalytic activity for the AZP sensor. In the presence of AZP, the EuO/GCE, g-CN/GCE, and EuO/g-CN/GCE exhibited enhanced reduction peaks; a considerable current response (-4.50 µA) was found at around -0.70 V for EuO/GCE, indicating that the EuO had a significant electrocatalytic activity for AZP reduction [39]. Also, cathodic peak current was observed in g-CN/GCE at a peak potential of -0.66V (-5.0 µA), indicating that g-CN has a large surface area and significant electrocatalytic activity for AZP reduction. In addition to that, different electrochemical active sites can be created by the non-bonding electrons in present in the nitrogen atom which can enhance the electrochemical reduction of AZP [40]. As expected, EuO/g-CN/GCE exhibits a higher reduction peak current ($E_{pc}$: -0.65 V, $I_{pc}$: -5.8 µA) due to synergetic effect between the g-CN flakes and EuO coral particles. The EuO/g-CN/GCE shows enhanced electrocatalytic activity in presence of AZP with a drastically improved current response that is nearly 1.42, 1.26, and 1.14 times that of bare GCE, g-CN/GCE, and EuO/GCE respectively (Fig. 4C). This higher current response due to the synergistic interaction, i.e., electron transfer between the conduction

band of the metal oxide and valance band of the graphitic carbon nitride, increase the charge transfer on the electrode surface which facilities the electrocatalytic activity towards AZP [41]. The modified and unmodified electrodes show major cathodic peak in the forward scan and a small anodic peak during the reverse scan around +0.2 V. The cathodic peak corresponds to the electrochemical reduction of nitro (AZP-$NO_2$) group to the respective hydroxylamine (AZP-NHOH). The anodic peak due to the electrocatalytic conversion of hydroxylamine to the respective nitroso group (AZP-NO) [42]. The corresponding electrocatalytic reduction of AZP on EuO/g-CN/GCE was schematically represented in

**Scheme 2**.

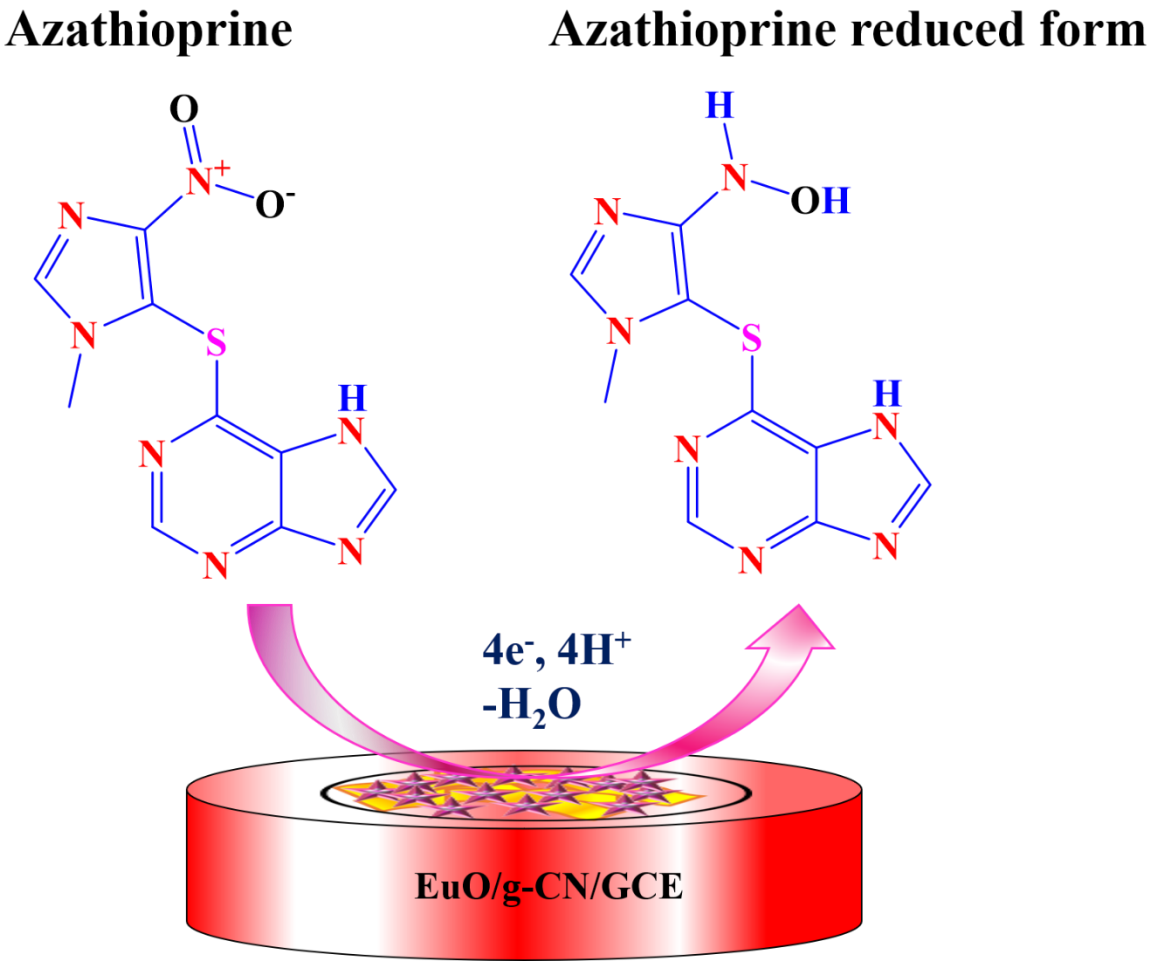


**Scheme 2.** Schematic representation of AZP reduction on EuO/g-CN/GCE

The Fig. 4D exhibits the concentration effect of AZP on EuO/g-CN/GCE. From that, raising the concentration of AZP, the peak current was heightened with respect to the concentration of AZP. The peak current was increased linearly from the lower concentration to higher concentration (25-150 µM). The respective linear plot was portrayed in Fig. 4F and a linear correlation equation, $I_{pc}$ (µA) = -0.034 (µM) -1.832, ($R^2$ = 0.99). From the above results, the electrocatalytic reduction of AZP at EuO/g-CN/GCE is a first-order kinetics, i.e., the reduction of AZP is concentration depending process. g-CN

has numerous electrons, many defects and a number of N atoms, therefore it could provide a variety of ionic adsorption centres. Moreover, due to the higher electronegativity of nitrogen atoms in the carbon nitride layers, different active sites (positive and negative sites) can be formed, which improves the wettability of the electrode surface and increases the adsorption of target molecules (AZP). Moreover, g-CN can be coupled with EuO, resulting in an electric field, which is an important driving force for ion transport between metal oxide and g-CN, leading to an enhancement of the catalytic activity of EuO/g-CN/GCE [41].

### *3.6. pH studies*

To analyse the pH effect of the AZP on EuO/g-CN/GCE, CV was carried out in 0.1 M PBS with different pH which containing 100 µM AZP. Fig. 5A exhibits the CVs of different pH of (3.0, 5.0, 7.0, and 9.0) the electrolyte at a 50 mV/s sweep rate, increasing current response was observed from pH 3.0 to 7.0. In contrast, the decreased current response was observed at pH

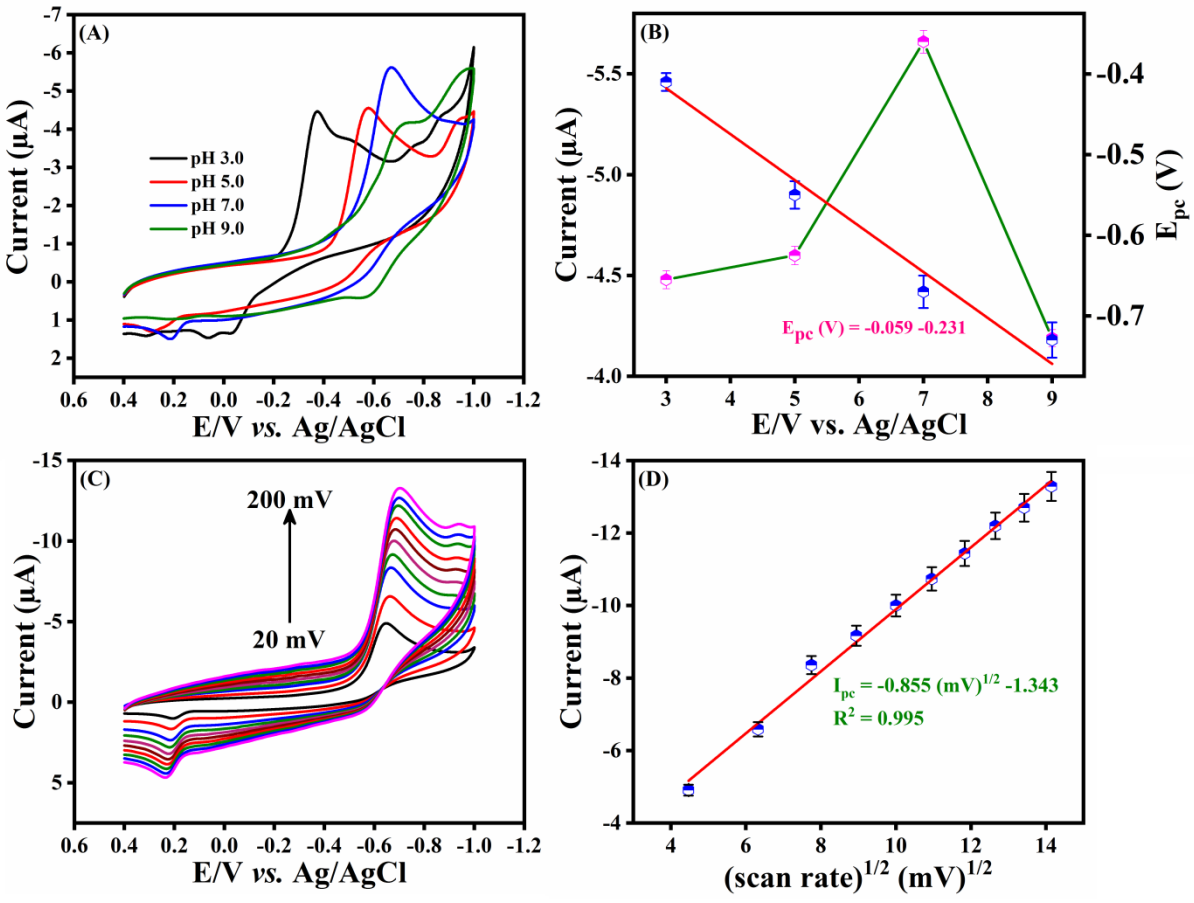


**Figure 5.** (A) CVs of EuO/g-CN/GCE at 50 mV/s sweep rate in different pH solutions, it consists 100 µM AZP. (B) Compression of reduction current of AZP with respect to the different pH (green line), and linear dependency between pH *vs.* peak potential (red line). (C) CVs on EuO/g-CN/GCE for 100 µM of AZP in 0.1 M PBS at different scan rate (20-200 mV/s). (D) Linear correlation diagram between $v^{1/2}$ vs. $I_{pc}$.

9.0. **Fig. 5B** (green line) demonstrates the AZP current response comparison with respect to the pH of the electrolyte. On that, higher current response was observed in pH 7.0. This behaviour of decreased current response at lower and higher pH is due to the presence of higher $H^+$ and $OH^-$ ions, they will influence the stability of electrode material as well as the electrochemical properties of AZP and decrease the current response. Subsequently, pH 7.0 was used as a suitable electrolyte in further electrochemical experiments. Notably, the reduction potential of AZP was shifted to more negative during the changing of pH from lower to higher (pH: 3.0 to 9.0), implies that protons were involved in the electrochemical reduction of AZP. In addition to that, linear dependency was observed between the reduction peak potential of AZP *vs.* pH of the electrolyte solution (Figure 6B; Red line) with a slope of 0.059 which agree with the theoretical value of 0.059 V/pH, demonstrated that protons and electrons were equally participate during the electrocatalytic reduction of AZP EuO/g-CN/GCE.

### *3.7. Scan rate studies*

CV was accomplished on EuO/g-CN/GCE with different scan rate to explore the effect of scan rate. **Fig. 5C** exhibits the CV histograms of 100 µM AZP in 0.1 M PBS with different scan rate. The reduction peak current of AZP was enhanced linearly respect with increasing scan rate from 20 to 200 mV/s. In addition, the peak potential was shifted towards negative potential when an increasing the scan rate. A linear correlation was observed between the reduction peak current of AZP vs. Square root of scan rate and the respective linear plot was showed in **Fig. 5D** along with the linear regression equation $I_{pc}$ (µA) = -0.855 $(mV)^{1/2}$ -1.343 ($R^2$ = 0.995), suggested that, the electrochemical reduction of AZP on EuO/g-CN/GCE is a diffusion-controlled process.

### *3.8. Analytical performance of EuO/g-CN/GCE for AZP*

For the determination of AZP based on EuO/g-CN/GCE, DPV was carried out for the different concentration of AZP in 0.05 M PBS (pH 7.0). The selected potential window for the DPV experiment was -0.2 to -1.0 V and the DPV curves of different concentration of AZP are shown **Fig. 6A.** The DPV current exhibits the steady increasing manner with respect to the concentration of AZP from 0.01 - 427.51 µM. Moreover, two linear ranges were achieved to the AZP peak current**. Fig. 6B** displays the calibration plot with two linear ranges and the first one from 0.01- 12.51 µM, respective with the linear regression equation of $I_{pc}$ (µA) = 0.173 C(µM) +1.186 ($R^2$ = 0.981) and. The second linear range was obtained from 18.51 - 427.51 µM, and the calibration equation is $I_{pc}$ = 0.019 C (µM) +4.012 ($R^2$ = 0.940). The lower detection limit efficiency, sensitivity of the EuO/G-CN/GCE was determined using the slope obtained from the first linear range. According to following Eqn-1, the LOD of AZP on EuO/G-CN/GCE was calculated as 0.008 µM.

LOD = 3S/B ……. (Eqn-1)

In Eqn-1, ‘S’ is the standard deviation of 3 blank DPV curves and ‘B’ is the slope obtained from the first linear range. Moreover, the sensitivity of the EuO/g-CN/GCE sensor was calculated as 0.41 µA

$\mu M^{-1}$ $cm^{-2}$. The obtained analytical parameters such as the linear ranges, sensitivity, and LOD of the assembled EuO/g-CN/GCE sensor towards AZP was compared with the previously reported AZP sensor using different electrodes and analytical techniques and they were listed out in the following **Table 1**. From that, the developed EuO/g-CN/GCE have a wide linear range, higher sensitivity with lower detection limit, demonstrated that EuO/g-CN/GCE is an essential material for the determination AZP.

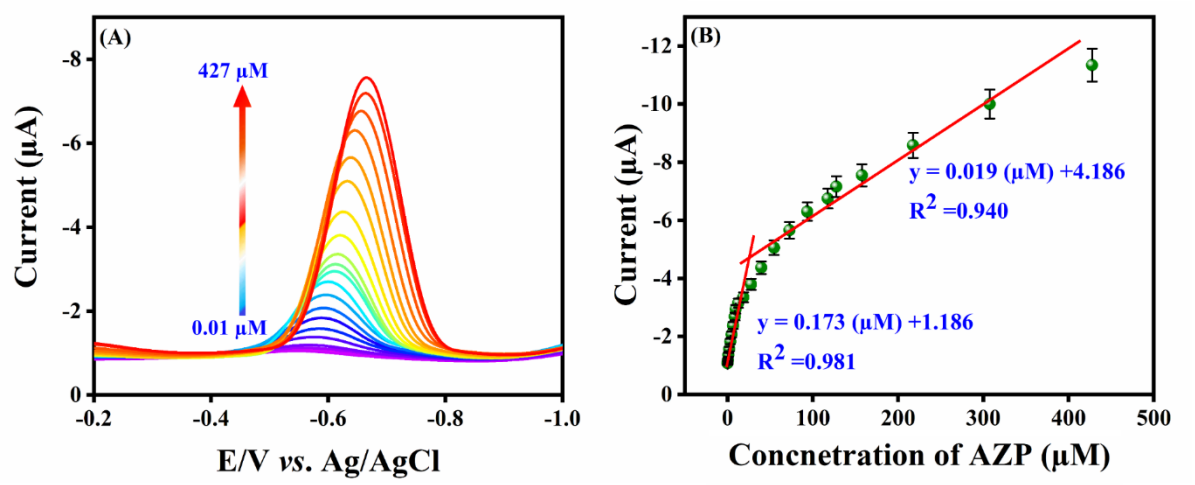


**Figure 6 (A)** DPVs on EuO/g-CN/GCE for different concentration of AZP (0.02 to 427 µM). **(B)** Correlation plot: AZP current *vs.* concentration of AZP.

*3.9. Repeatability, reproducibility, interference, and stability studies.*

The sensor's repeatability was then determined by measuring the current response to ten repeated DPVs in 0.1 M PBS (pH 7) containing 200 µM AZP. As illustrated in Fig. 7A, AZP reduction peak currents remained within 97.6% of their initial current values with a relative standard deviation (RSD) of approximately 1.05 percent for the EuO/g-CN-modified electrode, indicating that the electrodes are repeatable. DPV response to 200 µM AZP was accounted for the reproducibility analysis on EuO/g-CN modified electrode. Five distinct EuO/g-CN modified electrodes were constructed using the same process. The results were shown in Fig. 7B, illustrate that there is no detectable reduction in the reduction peak current of AZP, suggesting that the changed electrodes have a high degree of repeatability, as indicated by the calculated RSD value of around 1.23 percent. Moreover, EuO/g-CN/GCE demonstrated exceptional stability, reproducibility, and repeatability in determining AZP

Selectivity is a significant parameter for the electrochemical sensors. DPV was used to determine the effect of electroactive species like glucose [Glu], fructose [Fru], ascorbic acid [AA], $Mn^{2+}$, $Fe^{2+}$, $Ni^{2+}$, Nitrofurantoin [NFT], and hydroquinone [HQ] on EuO/g-CN/GCE for AZP sensing. Even though, the addition of 3-fold excess of interferes had no significant effect on the current response of 200 µM AZP (Fig. 7C). These findings validate that the proposed sensor is capable of detecting AZP in the presence of interfering species at large concentrations. Thus, great precision is used to validate the selectivity.

**Table 1.** Electrochemical determination of AZP based on different electrodes.

| S. No | Electrode | Technique | Linear (µM) | LOD (µM) | Reference |
|---|---|---|---|---|---|
| 1 | NDG/CS/GCE[a] | CV | 0.2 - 100 | 0.065 | [3] |
| 2 | Ag-NPs/PGE[b] | CV | 0.1-100 | 0.068 | [4] |
| 3 | Au NNs/GCE[c] | DPV | 0.5 - 2300 | 0.033 | [11] |
| 4 | Au/Au-NA[d] | DPV | 0.095-900 | 0.090 | [43] |
| 5 | CNP/N/GCE[e] | CV | 0.2-50 | 0.080 | [44] |
| 6 | EuO/g-CNk/GCE[f] | DPV | 0.02 - 427 | 0.008 | This work |

**a-** Nano-Diamond/Graphite/Chitosan/GCE
**b-** Silver nanoparticles/ Pyrolytic graphite electrode
**c-** Gold Neuronal like structure/GCE
**d-** Gold dendrites
**e-** Carbon nanoparticle/ Nafion film/GCE
**f-** Europium oxide/graphitic carbon nitride/GCE

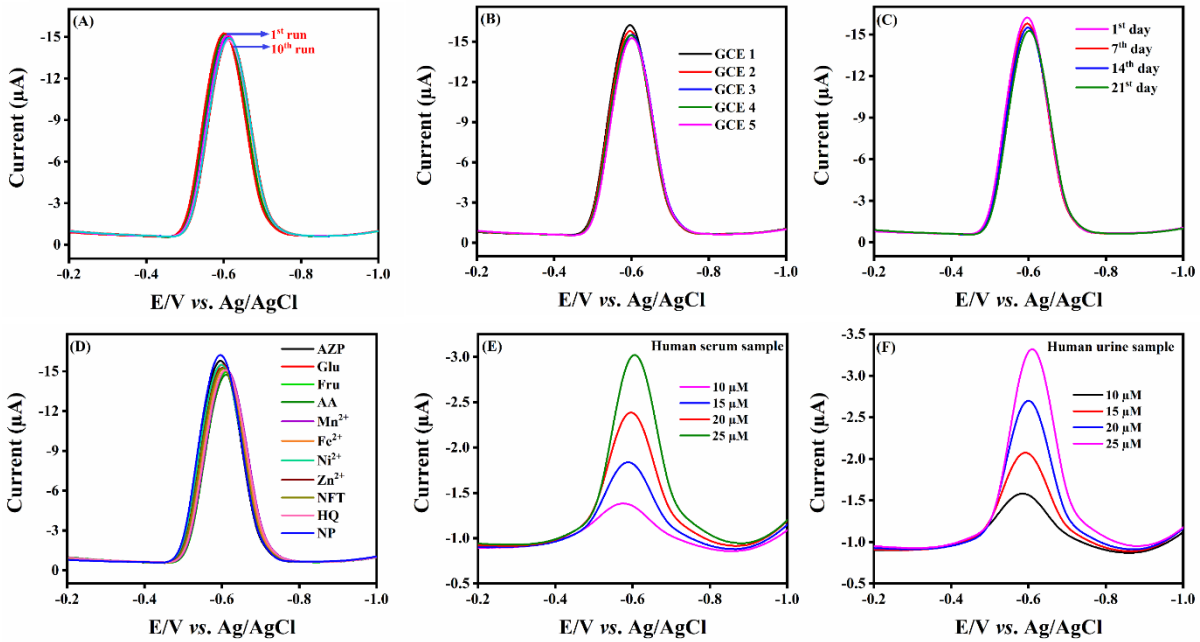


**Figure 7.** (A) DPV signal of repeatability study of 10 runs in the presence of 200 µM of AZP. (B) DPV signal of reproducibility of different GCE in identical conditions. (C) DPV signal of storage stability from 1 to 21st day in the presence of 200 µM of AZP. (D) DPV signal of selectivity study of AZP with various interfering species. (E, F) DPV signal of real sample analysis (human blood serum and urine samples).

To determine the sensor's stability, EuO/g-CN/GCE electrodes were stored in air at room temperature for 20 days and the CV response current of an electrode was recorded every 5 days. Over a period of 20 days, the electrode-maintained 98.5 percent of its original response current toward 200 µM of AZP (Fig. 7D). These findings support the proposed EuO/g-CN/GCE-based AZP sensor's excellent storage stability.

### *3.10. Real sample analysis*

To analyse the practical application of the as-prepared electrochemical sensor, DPV was carried out in real samples such as human urine sample, and blood serum. The required real samples were collected from medical hospital in Taiwan. The acquired real samples were centrifuged at 6000 rpm. The supernatant was collected and mixed with 5x PBS (0.1 M, pH 7.0) and identified as a stock solution.

**Table 2.** Achieved recovery results for AZP determination in real sample analysis (Blood serum, and urine sample) on EuO/g-CN/GCE.

| Sample | Added (µM) | Found (µM) | Recovery (%) |
|---|---|---|---|
| **Blood serum** | 10.0 | 9.7 | 97 |
| | 15.0 | 15.0 | 100 |
| | 20.0 | 19.8 | 99 |
| | 25. | 24.0 | 96 |
| **Urine sample** | 10. | 9.9 | 99 |
| | 15. | 14.4 | 96 |
| | 20. | 19.2 | 96 |
| | 25. | 24.8 | 99 |

To introduce the AZP into the stock solution, a known amount (1;1, Stock solution: AZP) of AZP was introduced into the stock solution, and directly used in the DPV experiments by the standard addition method. DPV experiment was performed in 0.1 M PBS with the potential window between -0.2 to -1.0 V. Fig. 7E, F exhibits the DPV curves performed in the real samples for a known concentration of AZP. The reduction peak current of AZP in real samples were similar to the DPV curves those were recorded in 0.1 M PBS. The AZP reduction peak current of AZP was linear increased during the increasing concentration. In addition to that, a good recovery results were obtained in both two real samples and which were listed in **Table 2.**

## 4. CONCLUSION

In conclusion, EuO/gCN composites was synthesized by utilizing a simple sonochemical process, and their applicability to the detection of AZP was investigated. The flake-like g-CN increases the conductivity of the EuO nanoparticle and thus its electrocatalytic activity toward AZP reduction. EuO/g-CN/GCE has a low LOD (8 nM) and high sensitivity for measuring AZP. The as-developed AZP sensor revealed the good repeatability, a fine reproducibility, and stability, with obtained accepted RSD values. Additionally, the real-time analysis of AZP in real samples such as human blood serum and urine samples was exhibited with good recovery results.

DECLARATION OF COMPETING INTEREST

The authors declare that they have no known competing financial interests or personal relationships that could have appeared to influence the work reported in this paper.

ACKNOWLEDGMENTS

The authors acknowledge the Ministry of Science and Technology (MOST 110-2113-M-027-003), Taiwan. This work is also jointly supported by projects from NTUT-NJUST-111-01 and NSFC51872141, National Taipei University of Technology, and Nanjing University of Science and Technology.

## References

1. R. L. Simmons, D. M. Canafax, D. S. Fryd, N. L. Ascher, W. D. Payne, D. E. Sutherland, J. S. Najarian, *Transplant Proc*. 2 (1986) 76-81
2. Y. Bouhnik, M. Lémann, J.Y. Mary, G. Scemama, R. Taï, C. Matuchansky, R. Modigliani, J.C. Rambaud, *Lancet*, 347 (1996) 215–219.
3. S. Shahrokhian, M. Ghalkhani, *Electrochim. Acta*, 55 (2010) 3621–3627.
4. E. Asadian, A. Iraji Zad, S. Shahrokhian, *Mater. Sci. Eng. C*, 58 (2016) 1098–1104.
5. S.P. Chen, Z. Qiao, A. Vivoni, C.M. Hosten, *Spectrochim. Acta - Part A Mol. Biomol. Spectrosc.*, 59 (2003) 2905–2914.
6. A. Shafaati, B.J. Clark, *Drug Dev. Ind. Pharm.*, 26 (2000) 267–273.
7. T.T. Fazio, A.K. Singh, E.R.M. Kedor-Hackmann, M.I.R.M. Santoro, *J. Pharm. Biomed. Anal.*, 43 (2007) 1495–1498.
8. N.G. Göger, H.K. Parlatan, H. Basan, A. Berkkan, T. Özden, *J. Pharm. Biomed. Anal.*, 21 (1999) 685–689.
9. J. Wang, P. Zhao, S. Han, *J. Chinese Chem. Soc.*, 59 (2012) 239–244.
10. K. Balamurugan, R. Rajakumaran, S.M. Chen, T.W. Chen, P.J. Huang, *Int. J. Electrochem. Sci.*, 16 (2021) 1–20.
11. L.P. Mei, J.J. Feng, S.S. Huang, Y.C. Shi, A.J. Wang, *Sensors Actuators, B Chem.*, 240 (2017) 996–1002.
12. Z. Xie, Q. Liu, Z. Chang, X. Zhang, *Electrochim. Acta*, 90 (2013) 695–704.
13. Y. Yanagisawa, R. Piao, S. Iguchi, H. Nakagome, T. Takao, K. Kominato, M. Hamada, S. Matsumoto, H. Suematsu, X. Jin, M. Takahashi, T. Yamazaki, H. Maeda, *J. Magn. Reson.*, 249 (2014) 38–48.
14. M. Nyman, M.A. Rodriguez, L.E. Shea-Rohwer, J.E. Martin, P.P. Provencio, *J. Am. Chem. Soc.*, 131 (2009) 11652–11653.
15. Y. Yan, X. Jia, Y. Yang, *Catal. Today*, 259 (2016) 292–302.
16. Y. Yan, K. Li, L. Thia, Y. Dai, J. Zhao, X. Chen, Y. Yang, J.M. Lee, *Environ. Sci. Nano*, 3 (2016)

701–706.
17. J. Zhou, J. He, T. Wang, X. Chen, D. Sun, *Electrochim. Acta*, 54 (2009) 3103–3108.
18. F. Dong, X. Xiao, G. Jiang, Y. Zhang, W. Cui, J. Ma, *Phys. Chem. Chem. Phys.*, 17 (2015) 16058–16066.
19. S. Tanaka, H. Ogasawara, K. Okada, A. Kotani, *J. Phys. Soc., Japan* 64 (1995) 2225-2232.
20. F. Xi, D. Zhao, X. Wang, P. Chen, *Electrochem. Commun.*, 26 (2013) 81–84.
21. C.-F. Lin, C.-H. Wang, W.-Y. Liao, T.-C. Chou, G.-B. Lee, *Micro Nano Lett.*, 1 (2006) 29.
22. C.F. Lin, G. Bin Lee, C.H. Wang, H.H. Lee, W.Y. Liao, T.C. Chou, *Biosens. Bioelectron.*, 21 (2006) 1468–1475.
23. C. Wang, J. Li, X. Luo, J. Hui, X. Liu, J. Tan, X. Zhao, *J. Electroanal. Chem.*, 780 (2016) 147–152.
24. J. Tian, Q. Liu, A.M. Asiri, A.H. Qusti, A.O. Al-Youbi, X. Sun, *Nanoscale*, 5 (2013) 11604–11609.
25. N. Cheng, P. Jiang, Q. Liu, J. Tian, A.M. Asiri, X. Sun, *Analyst*, 139 (2014) 5065–5068.
26. W.J. Ong, L.L. Tan, S.P. Chai, S.T. Yong, A.R. Mohamed, *Nano Energy*, 13 (2015) 757–770.
27. F. Salehnia, M. Hosseini, M.R. Ganjali, *Microchim. Acta*, 184 (2017) 2157–2163.
28. Q. Zhao, H. Zhou, W. Wu, X. Wei, S. Jiang, T. Zhou, D. Liu, Q. Lu, *Electrochim. Acta*, 254 (2017) 214–222.
29. M. Vázquez-González, W.C. Liao, R. Cazelles, S. Wang, X. Yu, V. Gutkin, I. Willner, *ACS Nano*, 11 (2017) 3247–3253.
30. V.G. Pol, O. Palchik, A. Gedanken, I. Felner, *J. Phys. Chem. B*, 106 (2002) 9737–9743.
31. F. Frumosu, S.L. Iconaru, D. Predoi, *Dig. J. Nanomater. Biostructures*, 6 (2011) 1859–1865.
32. R. Srinivasan, N.R. Yogamalar, J. Elanchezhiyan, R.J. Joseyphus, A.C. Bose, *J. Alloys Compd.*, 496 (2010) 472–477.
33. R.D.L. Gaspar, I.O. Mazali, F.A. Sigoli, *Colloids Surfaces A Physicochem. Eng. Asp.*, 367 (2010) 155–160.
34. S. Velmurugan, T.C.K. Yang, *ACS Appl. Electron. Mater.*, 2 (2020) 2845–2856.
35. S. Balu, S. Velmurugan, S. Palanisamy, S.W. Chen, V. Velusamy, T.C.K. Yang, E.S.I. El-Shafey, *J. Taiwan Inst. Chem. Eng.*, 99 (2019) 258–267.
36. M. Chegeni, M. Mehri, S. Dehdashtian, *J. Mol. Struct.*, 1242 (2021) 130752.
37. D. Kim, Y.H. Jin, K.W. Jeon, S. Kim, S.J. Kim, O.H. Han, D.K. Seo, J.C. Park, *RSC Adv.*, 5 (2015) 74790–74801.
38. J. Anupriya, S.M. Babulal, T.W. Chen, S.M. Chen, J.V. Kumar, J.W. Lee, S.P. Rwei, J. Yu, R. Yu, C.Y. Hong, *Int. J. Electrochem. Sci.*, 16 (2021) 1–19.
39. U. Rajaji, S. Manavalan, S. Chen, M. Govindasamy, T. Chen, T. Maiyalagan, *Compos. Part B*, 161 (2019) 29–36.
40. J. Wang, H. Xu, X. Qian, Y. Dong, J. Gao, G. Qian, J. Yao, *Chem. - An Asian J.*, 10 (2015) 1276–1280.
41. J. Zou, S. Wu, Y. Liu, Y. Sun, Y. Cao, J.P. Hsu, A.T. Shen Wee, J. Jiang, *Carbon N. Y.*, 130 (2018) 652–663.
42. R. Rajakumaran, K. Balamurugan, S.-M. Chen, R. Sukanya, C.B. Breslin, *ACS Appl. Nano Mater.*, 4 (2021) 13048–13059.
43. R. Dehdari Vais, N. Sattarahmady, K. Karimian, H. Heli, *Sensors Actuators, B Chem.*, 215 (2015) 113–118.
44. S. Shahrokhian, M. Ghalkhani, *Electrochem. Commun.*, 11 (2009) 1425–1428.